High-Performance Mesoporous Bioceramics Mimicking Bone Mineralization

Isabel Izquierdo-Barba,[†,‡] Daniel Arcos,[†,‡] Yasuhiro Sakamoto,[§] Osamu Terasaki,[§] Adolfo López-Noriega,[†,‡] and María Vallet-Regí*[,†,‡]

Departamento de Química Inorgánica y Bioinorgánica, Facultad de Farmacia, Universidad Complutense de Madrid, 28040 Madrid, Spain, Centro de Investigación Biomédica en Red. Bioingeniería, Biomateriales, y Nanomedicina, CIBER-BBN, Spain, and Department of Structural Chemistry, Arrhenius Laboratory, Stockholm University, S-10691, Stockholm, Sweden

Received January 17, 2008. Accepted February 12, 2008

The preparation of bioceramics with ordered mesoporous structures is of importance for biomedical technology, for the design of bone and dental grafts with regeneration purposes. Here we demonstrate that hexagonal mesoporous $SiO_2-CaO-P_2O_5$ bioglasses (MBG) with high calcium content are the first known bioceramics that exhibit amorphous calcium phosphate (ACP)−octacalcium phosphate (OCP)−calcium deficient carbonatehydroxyapatite (CDHA) maturation as biomineralization governing mechanism in simulated body fluid (SBF), similarly to the in vivo biomineralization process. The unique characteristics of hexagonal MBGs lead to a local acid pH at the bioceramic surface that allows the formation of metastable OCP. Besides, 3D cubic MBG has been also synthesized, exhibiting higher surface area and porosity. The 3D reconstruction carried out by electron microscopy evidence a 3D bicontinuous network comprising a pair of rods mutually intertwined, creating the pore system available in three dimensions. This 3D pore system provides not only high surface area and porosity but also easier interchange of ions, increasing mass transport and diffusion processes. The final result is that 3D cubic MBGs exhibit an accelerated bioactivity behavior, forming a bonelike apatite phase on the surface, 1 h after coming into contact with SBF.

Introduction

During the last decades, the development of bioactive materials for hard tissue replacement has allowed important advances in the field of bone and dental grafting.[1,2] These materials exhibit highly reactive surfaces able to bond to the living tissues. The link is named bioactive bond, which is initiated through the nucleation and growth of an apatite-like phase at the implant−tissue interface. The newly formed apatite, together with the adsorption of biological moieties, constitutes an excellent layer for the action of osteoblasts and the subsequent bone-implant fixation.[3]

Currently, the challenges go further than just ensuring the implant-bone fixation. The development of surfactant-templated chemical routes allows the synthesis of materials with the control of surfaces at the nanoscale level, thus enabling to mimic the biomineralization process and stimulating the osteoblast function for regenerative purposes.[4–6] In other words, it is not about substituting the bone but supplying a graft that stimulates the bone regeneration. One of the most interesting approaches to this aim is tailoring grafts exhibiting two characteristics. First, the material should mimic as much as possible the biomineralization, thus cooperating at the natural healing processes. Second, the graft should be able to improve the healing rate, accelerating the natural healing processes and therefore reducing the post operative periods. Materials having these characteristics would also exhibit excellent properties as scaffolds for bone tissue engineering, where the osteblasts must be stimulated to form bone tissue under in vitro conditions prior to be implanted in vivo.[7,8]

In the last 15 years, the application of amphiphilic molecules for using their structure directing features at the SiO_2 systems has resulted in a new generation of mesoporous materials for catalysis, sensors, laser, and other technological purposes.[9,10] After considering the excellent textural properties of these molecular sieves, the research group of Zhao[11] and our group[12] separately decided to use this kind of synthetic route, to obtain biocompatible $SiO_2-CaO-P_2O_5$ systems through the evaporation-induced self-assembly (EISA) method.[13] This method allows the synthesis of

* Corresponding author. Phone: 34 91 3941870. Fax: 34 91 3941786. E-mail: vallet@farm.ucm.es.
† Universidad Complutense de Madrid.
‡ CIBER-BBN.
§ Stockholm University.

(1) Hench, L. L.; Wilson, J. *Science* **1984**, *226*, 630–636.
(2) Hench, L. L.; Polak, J. *Science* **2002**, *295*, 1014–1017.
(3) Vallet-Regí, M. *Dalton Trans.* **2006**, (44), 5211−5220.
(4) Ben-Nisan, B. *MRS Bull.* **2004**, *29*, 28–32.
(5) Webster, T. J.; Ergan, C.; Doremus, R. H.; Siegel, R. W.; Bizios, R. *Biomaterials* **2000**, *21*, 1803–1810.
(6) Vallet-Regí, M. *Chem.−Eur. J.* **2006**, *12*, 5934–5943.
(7) Langer, R.; Vacanti, J. P. *Science* **1993**, *260*, 920–926.
(8) Anselme, K. *Biomaterials* **2000**, *21*, 667–681.
(9) Kresge, C. T.; Leonowicz, M. E.; Roth, W. J.; Vartuli, J. C.; Beck, J. S. *Nature* **1992**, *359*, 710–712.
(10) Davis, M. E. *Nature* **2002**, *417*, 813–821.
(11) Yan, X. X.; Yu, C. Z.; Zhou, X. F.; Tang, J. W.; Zhao, D. Y. *Angew. Chem., Int. Ed.* **2004**, *43*, 5980–5984.
(12) López-Noriega, A.; Arcos, D.; Izquierdo-Barba, I.; Sakamoto, Y.; Terasaki, O.; Vallet-Regí, M. *Chem. Mater.* **2006**, *18*, 3137–3144.
(13) Brinker, C. J.; Lu, Y. F.; Sellinger, A.; Fan, H. Y. *Adv. Mater.* **1999**, *11*, 579–585.

10.1021/cm800172x CCC: $40.75
Published on Web 04/19/2008

Table 1. Nominal Composition, Textural and Structural Parameters Obtained by N_2 Adsorption, X-ray Diffraction, and Transmission Electron Microscopy, Corresponding to Ordered Mesoporous Glasses

sample	nominal composition	surface area[a] ($m^2\ g^{-1}$)	pore volume[b] ($cm^3\ g^{-1}$)	pore diameter[b] (nm)	symmetry	unit cell[c] (Å)	unit cell[d] (Å)
S58m	58%SiO_2-37%CaO-5%P_2O_5	195 (95)	0.46 (0.35)	9.45	*p6 mm*	79.2	76.2
S85m	85%SiO_2-10%CaO-5%P_2O_5	427 (227)	0.45 (0.24)	5.05	$Ia\bar{3}d$	180	172

[a] Calculated by the BET method. Values in bracket correspond to the textural values obtained for conventional sol−gel glasses with analogous compositions (refs 21, 22). [b] Calculated from the adsorption branch of N_2 isotherm using the BJH method. Values in bracket correspond to the textural values obtained for conventional sol−gel glasses with analogous compositions (refs 21, 22). [c] Calculated from the XRD pattern. [d] Calculated from Fourier diffractogram.

ordered mesoporous structures that evolve from hexagonal phases to cubic ones as a function of CaO content. Here, we show that these bioceramics exhibit the first evidence of amorphous calcium phosphate (ACP)−octacalcium phosphate (OCP)−calcium deficient carbonate hydroxyapatite (CDHA) maturation stages as governing mechanism. The natural calcium phosphate (CaP) maturation, suspected by many researchers,[14–16] has finally been observed in the laboratory through HRTEM studies on mesoporous bioactive glasses (MBG) by soaking in simulated body fluid (SBF). Moreover, the possibility of tailoring the structural characteristics of mesoporous glasses have allowed us to obtain bioceramics with 3D cubic bicontinuous structure, which permits higher accessibility of pore systems exhibiting the most accelerated bioactive process until now described.

Experimental Section

Synthesis and Characterization. Two highly ordered mesoporous $SiO_2-P_2O_5-CaO$ sol−gel glasses were synthesized by using a nonionic surfactant Pluronic P123 (BASF) as structure directing agent and evaporation-induced self-assembly (EISA) process (Table 1). Tetraethyl orthosilicate (TEOS), triethyl phosphate (TEP), and calcium nitrate, $Ca(NO_3)_2 \cdot 4H_2O$ (Aldrich) were used as SiO_2, P_2O_5 and CaO sources, respectively, as described in a previous paper.[12] The structural and textural characterization was performed by Powder X-ray diffraction (XRD) in a Philips X'Pert diffractometer equipped with a Cu Kα radiation (wavelength 1.5406 Å), by nitrogen adsorption porosimetry in a Micromeritics ASAP 2010 and by transmission electron microscopy (TEM) in a JEOL 3010 electron microscope operating at 300 kV (Cs; 0.6 mm, resolution 1.7 Å). All TEM images were recorded using a CCD camera (MultiScan model 794, Gatan, 1024 × 10 24 pixels size 24 μm × 24 μm) using low-dose condition. Fourier transform (FT) patterns have been conducted using Digital Micrograph (Gatan). To have a higher knowledge about the structural characteristic, we have performed a 3D reconstruction of such synthesized MBG from HRTEM images and by using an electron crystallography technique that provides a detailed structure of the inside of the mesoporous crystal, such as diameter, shape, and connectivity of the pores.[17,18]

In vitro Bioactivity Assessments. Two parallel assessments of in vitro bioactivity were performed in presence and absence of serum proteins in simulated body fluid (SBF) which has similar composition and ionic concentrations to those of human plasma.[19]

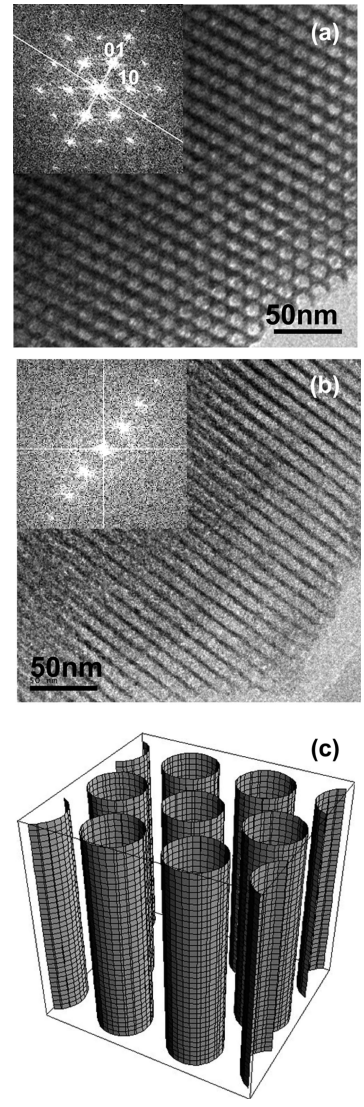

Figure 1. TEM images and Fourier patterns of S58m obtained along the (a) [0 0 1] and (b) [1 0 0] directions; (c) scheme representing the array of parallel channels along the *c* axis of this mesostructure.

For these purposes, a series of 200 mg of glass powder was soaked in 50 mL of serum-free SBF, whereas a second series was soaked into SBF supplemented with 20% of fetal bovine serum (FBS). Both experiments were carried out in polyethylene containers at 37 °C, under sterile conditions and continuous stirring. After different time periods, mesoporous glass powders were filtered and rinsed with distilled water, ethanol, and finally dried at room temperature. To compare the protein adsorption capacity, we have also studied conventional sol−gel glasses of analogous composition by soaking it in SBF supplemented with 20% FBS under the same conditions. The changes occurred onto the MBGs surface as a function of soaking time in SBF were studied by pH measurements evolution in both SBF and glass surface, Fourier transform infrared

(14) Brown, W. E.; Eidelman, N.; Tomazic, B. *Adv. Dent. Res.* **1987**, *1*, 306–313.
(15) Bodier-Houlle, P.; Steuer, P.; Voegel, J. C.; Cuisinier, F. J. G. *Acta Crystallogr., Sect. D* **1998**, *54*, 1377–1381.
(16) Nancollas, G. H.; Tomazic, B. *J. Phys. Chem.* **1974**, *78*, 2218–2225.
(17) Sakamoto, Y.; Kaneda, M.; Terasaki, O.; Zhao, D. Y.; Kim, J. M.; Stucky, G.; Shin, H. J.; Ryoo, R. *Nature* **2000**, *408*, 449–452.
(18) Sakamoto, Y.; Kim, T. W.; Ryoo, R.; Terasaki, O. *Angew. Chem., Int. Ed.* **2004**, *43*, 5231–5234.
(19) Kokubo, T.; Kushitani, H.; Sakk, S.; Kitsugi, T.; Yamamuro, T. *J. Biomed. Mater. Res.* **1990**, *24*, 721–734.

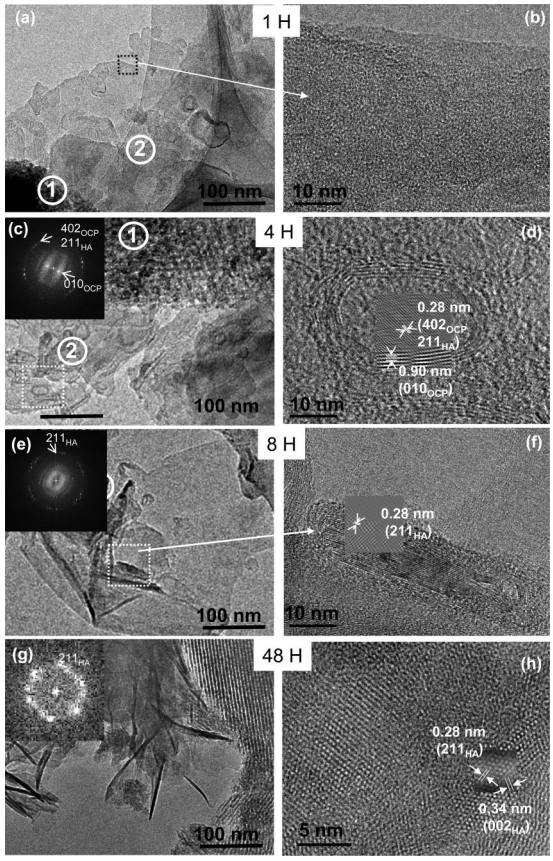

Figure 2. TEM images of S58m after being soaked in SBF at different times: (a, b) 1 h in SBF; a large amount of ACP is observed next to MBG grain. (c, d) 4 h in SBF; nanometrical oval nuclei are observed within the ACP matrix; (d) higher-magnification evidence that these nuclei are nanocrystalline structures constituted by OCP and HA; (e, f) 8 h in SBF. Needle shaped apatite crystallizes within the ACP matrix. Magnified images (d) and (f) evidence the microstructural evolution of OCP nuclei to apatite crystallites. Ca/P ratios for the newly formed CaP are also shown.

(FTIR) spectroscopy (Nicolet Magma IR 550 spectrometer equipped with a Golden Gate accessory), and TEM in a JEOL 3000 FEG electron microscope fitted with a double tilting goniometer stage (±45°) and with a Oxford LINK EDS analyzer.

Results and Discussion

MBGs with 2D Hexagonal Structure. Figure 1 shows the highly ordered structure of a S58m MBG of composition SiO_2 (58)−CaO (36)−P_2O_5 (6) (mol %). The pores are ordered following a 2D hexagonal array with a unit cell of symmetry *p6mm*. This mesostructure leads to an array of parallel channels along the *c* axis (see Figure 1c), leading to surface area and porosity values significantly higher than those corresponding to conventional sol−gel glasses (Table 1 and supplementary data). The mesostructure imposed by the structure directing agent not only determines the textural properties, but also imposes a high chemical homogeneity. Conventional nonordered sol−gel glasses in the system SiO_2−CaO−P_2O_5 system commonly exhibit chemical and microstructural heterogeneity with small nuclei of crystalline calcium phosphate segregated out of the amorphous silica matrix.[20] Our MBG exhibit higher homogeneity degree in the pore wall, although nanocrystals, clusters, or CaP nuclei could exist within the mesostructure (see the Supporting Information).

Because of the open channel array, the high textural parameters and the relatively high CaO content, S58m MBG shows outstanding biomimetic behavior in contact with SBF. The biomimetic behavior can be monitored by HRTEM. Figure 2a shows the HRTEM images obtained from S58m after 1 h soaked in SBF. The MBG (site 1) appears covered by a large amount of newly formed calcium phosphate (site 2). Higher-magnification evidence the amorphous structure of this biomimetic CaP with Ca/P ratio of 1.22 (Figure 2b and Table 2). This step has been widely observed in many bioactive compositions[21–23] and corresponds to step 4 of the bioactive process described by Hench.[24] To date, the accepted mechanism involved the crystallization of a calcium-deficient carbonatehydroxyapatite (CDHA) from this amorphous calcium phosphate (ACP). However, the maturation occurred on S58m is different as can be seen in Figure 2c. After 4 h in SBF, the HRTEM image (Figure 2c) evidences the development of nanocrystalline oval nuclei of 12 nm in width and 18 nm in length within the ACP layer. A higher magnification (Figure 2d) evidence that these oval shaped nuclei show two d-spaces at 0.90 and 0.28 nm corresponding to the 010 and 402 reflection of an OCP-like phase. The d-value of 0.28 nm could also be assigned to the 211 reflections of an apatite like phase; however apatite-like phase does not have any d value around 0.9 nm, which evidence the presence of octacalcium phosphate (OCP) at this stage of the biomimetic process.[25] The Ca/P ratio is 1.35 (Ca/P ratio is 1.33 for OCP), in agreement with a biphasic nuclei constituted by OCP with a small fraction of HA. The transformation from oval OCP nuclei to needle shaped apatite nanocrystals is finally evident on MBG surfaces after 8 h (images e and f in Figure 2). These crystallites show *d*-spaces of 0.28 nm that could be assigned to the 211 reflection of an apatite-like phase together with an increase of Ca/P ratio up to 1.37 (see Table 2). Insofar the soaking time increases the OCP to CDHA transformation is confirmed. After 48 h in SBF, needle-shaped apatite crystals with a Ca/P molar ratio of 1.52 are clearly observed (Figure 2g,h). Note the stable mesoporous structure of MBG after 2 days in SBF, which is very important for their potential application as controlled delivery matrices and/or reservoir of bone regeneration factors.

Therefore, an ACP−OCP−CDHA maturation sequence is observed onto the MBG surface in contact with SBF which had never been observed before in any other bioactive ceramic. This physiological mechanism of natural bone was proposed by Brown and involves the growth of biological apatites from octacalcium phosphate which has a transitory existence.[14] This hypothesis is supported by the observation of an OCP "central dark line" in many biological apatites as

(20) Vallet-Regi, M.; Salinas, A. J.; Ramirez-Castellanos, J.; Gonzalez-Calbet, J. M. *Chem. Mater.* **2005**, *17*, 1874–1879.
(21) Vallet-Regí, M.; Ragel, C. V.; Salinas, A. J. *Eur. J. Inorg. Chem.* **2003**, (6), 1029−1042.
(22) Vallet-Regí, M.; Arcos, D.; Pérez-Pariente, J. J. *Biomed. Mater. Res.* **2000**, *51*, 23–28.
(23) Pereira, M. M.; Clark, A. E.; Hench, L. L. *J. Biomed. Mater. Res.* **1994**, *28*, 693–698.
(24) Hench, L. L., Anderssson, O. In *Bioactive Glasses. An Introduction to Bioceramics*; Hench, L. L. Wilson, J., Eds.; Elsevier Science: New York, 1995; p 477.
(25) Leng, Y.; Chen, J.; Qu, S. *Biomaterials* **2003**, *24*, 2125–2131.

Table 2. Ca/P Ratio Calcium Phosphate Phases Observed onto the MBG Surfaces As a Function of Soaking Time in SBF

	1 h		4 h		8 h		48 h	
	Ca/P	phases	Ca/P	phases	Ca/P	phases	Ca/P	phases
S58m	1.22	ACP	1.35	ACP OCP CDHA	1.37	ACP CDHA	1.52	CDHA[a]
S85m	1.37	ACP CDHA	1.42	ACP CDHA	1.50	ACP CDHA	1.62	CDHA

[a] A small fraction of ACP could be found.

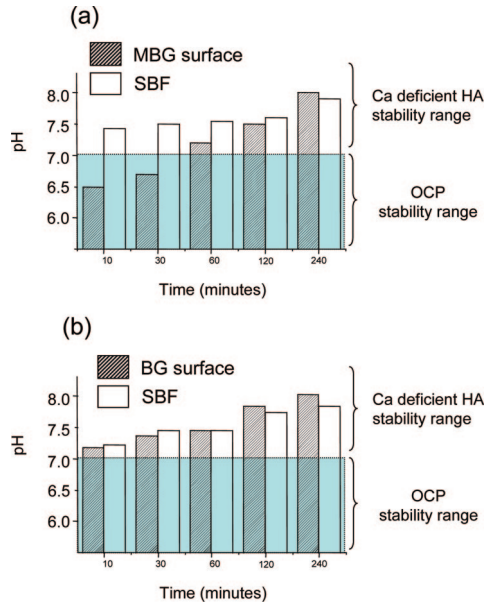

Figure 3. pH values as a function of time at the bioceramic surface and SBF: (a) for S58m mesoporous bioglass and (b) a conventional sol−gel glass with the same chemical composition. MBG surface shows acid pH during the first 30−45 min in SBF, whereas the SBF exhibit basic pH from the beginning of the experiment. Conventional sol−gel glass surface shows similar basic pH to SBF during the experiment. OCP and apatite stability ranges are shown.

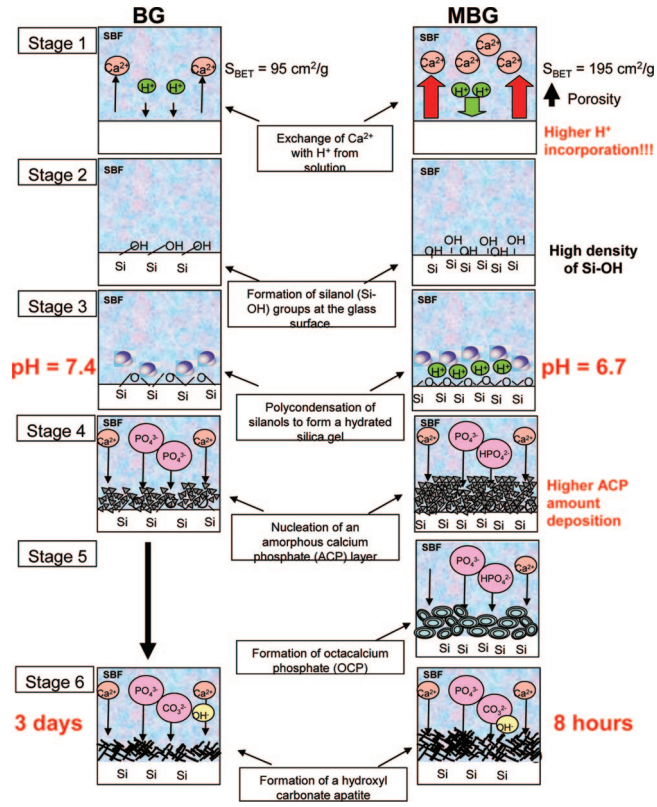

Figure 4. Bioactive mechanism in simulated body fluid of conventional sol−gel glasses (proposed by Hench in 1970) versus bioactive mechanism of mesoporous bioactive glasses proposed in this manuscript.

consequence of an incomplete hydrolysis of OCP.[15,16] OCP can be described as an alternating layer structure of an apatite layer and a hydrated layer, where the apatite layer is structurally very similar to apatite phase. According to the model proposed by Brown for in vivo conditions,[26] the first calcium phosphate crystals formed in a physiological supersaturated solution are OCP-like. The subsequent hydrolysis step leads to the formation of apatite phase. The OCP to apatite phase transformation has been described as a simple dehydratation process. Recently, Tseng et al.[27] have provided a deeper description for an in vitro system preparing OCP by mixing urea, sodium phosphate monobasic dehydrate, and calcium nitrate tetrahydrate at 100 °C. They find that the hydrolysis reaction of the PO_4^{3-} and HPO_4^{2-} ions is the key chemical reaction for OCP to HA transformation

$$HPO_4^{2-} + OH^- \rightarrow PO_4^{3-} + H_2O$$

However, this is the first time that OCP to CDHA transformation is observed in simulated physiological conditions (pH 7.4, similar ionic composition, 37 °C, etc.) onto a bioactive ceramic surface.

OCP is a metastable phase and will appear only if the pH in the crystallization system is below 7. This is not the pH condition of in vitro SBF systems (pH 7.2−7.4 that increases as a function of the soaking time) and it can explain the reason OCP has never been observed when conventional bioactive glasses were soaked in SBF. Therefore, the question is why OCP is observed during the biomimetic process in MBG, but not in conventional bioglasses. Figure 3a shows the pH evolution in the SBF and on S58m surface as a function of soaking time. The initial (before MBG soaking) pH of SBF is 7.4 and gradually increases as a function of soaking time. This pH evolution of the SBF is very similar in the case of conventional BG. In both cases, Ca^{2+} cations from the substrate are exchanged by H^+ from the SBF, with the subsequent pH increase in the fluid. However, the pH values on the substrates surfaces exhibit very important differences. Whereas the pH evolution of conventional BG is almost equivalent to the SBF, the pH of S58m exhibits values below 7 after 10 min in SBF. Only after 1 h, the surface of MBG reaches pH values above 7, that is, similar to those on the surrounding fluid. In the case of MBG, the large and accessible porosity, high surface area, and high material reactivity accelerate the ionic exchange, establishing

(26) Brown, W. E.; Nylen, M. U. *J. Dent. Res.* **1964**, *43*, 751.

(27) Tseng, Y. H.; Mou, C. Y.; Chan, J. C. C. *J. Am. Chem. Soc.* **2006**, *128*, 6909–6918.

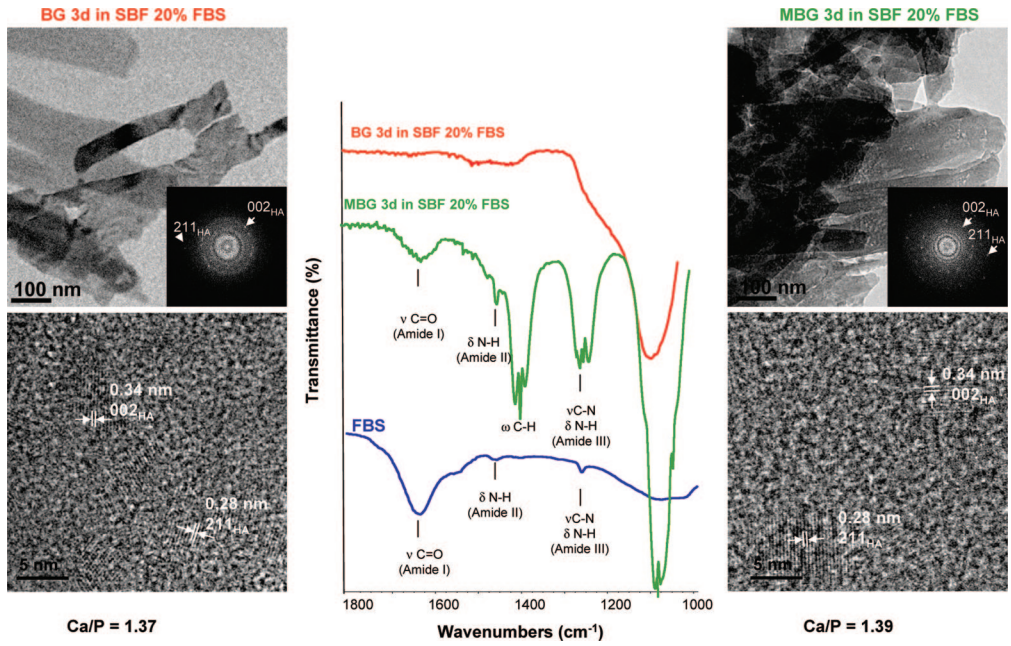

Figure 5. HRTEM images and their Fourier diffractograms. Left and right parts correspond to conventional BG and MBG after 3 days in SBF supplemented with 20% FBS, respectively. FTIR spectra corresponding to FBS solution, BG, and MBG glasses after 3 days in serum-supplemented SBF.

two different pH environments, as can be seen in Figure 3. In the case of S58m, the intensity of the $Ca^{2+}-H^{+}$ exchange results in a local acidic environment at the MBG surface (Figure 3a). This acidic environment probably corresponds to the acid gel of silica formed after condensation of silanol groups (stage 3 of Hench's theory). Subsequently, a large amount of ACP precipitates onto the acid surface as a result of the solution supersaturation and the high surface area available. Thereby, the acidic surface of the MBG becomes temporally isolated and allows the formation of OCP during the first hour, i.e., while the acid silica gel is not in contact with the external basic fluid. To the extent the soaking time increases, the transformation of OCP into CDHA takes place in terms explained above. By comparing images d and f in Figure 2, the transformation from oval OCP nuclei to needle-shaped apatite nanocrystals is evident.

On the contrary, this local acid pH does not occur in the surface of conventional bioglasses, whose surface exhibit the same basic media (pH 7.3 or higher) than the surrounding fluid from the beginning of the bioactive process (Figure 3b).

Summarizing, the resemblance between the in vivo calcium phosphate maturation and the in vitro biomimetism of MBG is closely related with compositions with relatively high Ca^{2+} content and high open porosity, which forces us to reformulate the bioactivity stages description in term of the unique physicochemical characteristics exhibit on MBG surface. The mechanism governing the CDHA layer formation onto the surface of MBG is similar to that proposed by Hench et al.[24] for conventional BG. However, there are important differences that lead to an accurate biomimetism in MBG respect to natural bone. Such differences are summarized in Figure 4 and can be described as follows:

Stage 1: Rapid exchange of Ca^{2+} with H^{+} from the solution (SBF). In the case of MBG, a high and accessible porosity, high surface area, and high material reactivity accelerate the surface processes, which permit a more intense ionic exchange and higher H^{+} incorporation compared with conventional BG.

Stage 2: Formation of silanol (Si-OH) groups at the glass surface. In the case of MBG a higher density of Si-OH groups occurs because of the higher surface area and larger H^{+} incorporation than conventional BG.

Stage 3: Polycondensation of silanol groups to form a hydrated silica gel. In the case of MBG, a highly protonated silica gel is formed after the condensation of silanol groups, leading to an acid local pH (pH 6.7) on the glass surface. On the contrary, this local acid pH does not occur at the surface of conventional BG, whose surface exhibit the same basic media (pH 7.4 or higher) than the surrounding fluid since the beginning of the bioactive process.

Stage 4: Nucleation of an amorphous calcium phosphate (ACP) layer. In the case of MBG, higher ACP precipitation occurs compared with that observed in conventional BG.

Stage 5: Crystallization of ACP by incorporation of Ca^{2+} and HPO_4^{2-} ions to form nuclei of octacalcium phosphate. The acidic surface of the MBG allows the formation of OCP during the first hours. Such a stage does not occur in conventional BG.

Stage 6: In the case of MBG, the maturation of OCP into calcium-deficient hydroxylcarbonate apatite (CDHA) takes place through a dehydratation process, which occurs only with small OCP crystallites; the hydrolysis reaction of the PO_4^{3-} and HPO_4^{2-} ions would be the key chemical reaction for OCP to CDHA transformation. In the case of conventional BG, a direct crystallization of previously precipitated ACP (stage 5) occurs by incorporation of OH^{-} and CO_3^{2-} ions to form HCA. The time period for the CDHA formation is very different in both glasses. In the case of conventional BG, the CDHA formation takes place after 3 days in SBF, whereas in the MBG it takes only 8 h.

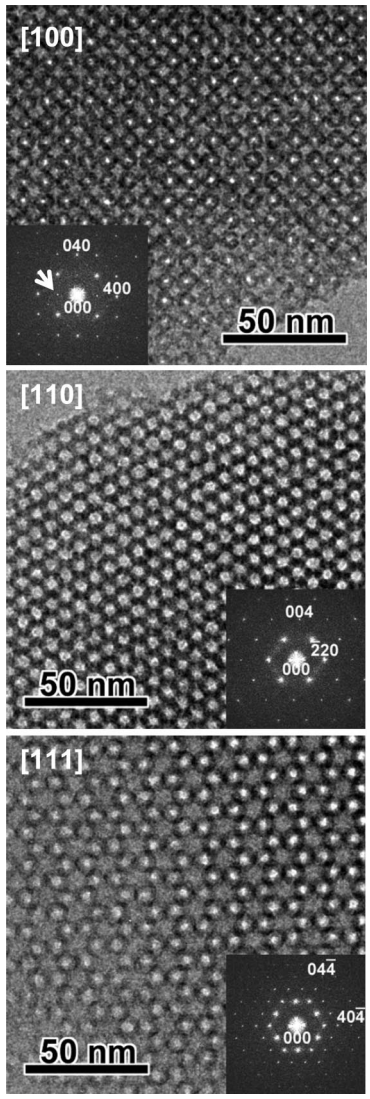

Figure 6. HRTEM images and their corresponding Fourier diffractograms of S85m sample taken with the incident beam parallel to the [100], [110], and [111] directions. The arrow indicates the presence of the 200 reflection (forbidden for $Ia\bar{3}d$ structure), which indicates a small deviation of such structure.

Moreover, an in vitro study in the presence of serum proteins has been performed in order to compare the protein surface adsorption capacity of MBG with conventional BG. Figure 5 shows the excellent protein adsorption of MBG compared with conventional ones when both ceramics are soaked in SBF containing 20% fetal bovine serum (FBS). The FTIR spectrum of MBG glass after 3 days in SBF supplemented shows the presence of bands at 1635, 1450, and 1395 cm^{-1} corresponding to amide I, amide II band, and amide III groups, respectively (these bands are also observed in the spectrum corresponding to the FBS solution), and a band at 1305 cm^{-1} corresponding to CH groups from glycoproteins of FBS. The presence of these bands indicates the proteins adsorption onto the MBG surface. In the case of conventional BG, its FTIR spectrum shows very weak bands corresponding to the protein adsorption. HRTEM images and EDS analyses show in both cases a large number of elongated precipitated composed with calcium and phosphorus (Ca/P ratio ca. 1.40) less regular and obviously thicker than those in vitro essays in SBF without any serum proteins. Fourier diffractograms show two visible rings corresponding to 002 and 211 reflections, indicating the formation of CDHA of small crystallites on their surface (see higher-magnification images).

MBG with 3D Cubic Structure. The new properties of MBG are not limited to accurately mimic the in vivo CaP maturation. Compositions with low CaO content in the $SiO_2-CaO-P_2O_5$ system possess a mesostructure consisting in a 3D cubic arrangement that leads to an extraordinary increment of the textural properties, with important consequences in the formation kinetic of the biomimetic apatite. For instance, the mesoporous structure of the material S85m, with composition SiO_2 (85)−CaO (10)−P_2O_5 (5) (mol %) (see Table 1) is shown in Figure 6. This figure shows the high resolution TEM (HRTEM) images and Fourier diffractograms viewing along the [100], [110] and [111] directions. HRTEM images and Fourier diffractograms show the same contrast as 3D-bicontinuous cubic with $Ia\bar{3}d$ symmetry which is observed in mesoporous crystals MCM-48 and FDU-5.[18,28] Therefore, in order to study the possible pore connectivity within this bioceramic we decided to carry out a 3D reconstruction, where the $Ia\bar{3}d$ space group was assumed. Images taken with the three different zone axes [100], [110], and [111] were used for the reconstruction process. 3D electrostatic potentials were calculated (Figure 7a), and together with the total pore volume value (0.45 cm^3/g), the glass mesoporous wall density (2.2141 g cm^{-3}), the 3D pore structure was determined (see the Supporting Information). Panels b and c in Figure 7 show the 3D pore structures with different orientations. Pore diameter and wall thickness values are 5.8 and 3.2 nm, respectively, which have been estimated by electron crystallography. The 3D pore reconstruction indicates that the glass wall follows the G-surface, which is composed of a bicontinuous 3D network.[18]

The structural characteristics of mesoporous glasses determine the textural values, thus having a great influence on the bioactive properties. Figure 8 shows the HRTEM images of the newly CaP phases formed on S85m during the first hours within SBF. Nanocrystalline apatite is observed after 1 h in SBF, evidencing the fastest apatite kinetic formation observed so far, for an in vitro biomimetic process (Figure 8a). A higher-magnification (Figure 8b) image shows the presence of ACP together with a nanocrystalline apatite-like phase. No OCP nuclei are observed on this sample. The Ca/P ratio (1.37) indicates that ACP predominates over apatite phase, because 1.37 is too low for a single Ca deficient apatite phase. After 4 h in SBF, the surface of S85m is mainly covered by needle-shaped apatite crystallites (Figure 8c), although a few ACP grains can be observed (Figure 8d). At this point, the Ca/P ratio is 1.42, indicating an evolution toward a single apatite-like phase by Ca^{2+} incorporation. After 8 h

(28) Kaneda, M.; Tsubakiyama, T.; Carlsson, A.; Sakamoto, Y.; Oshuna, T.; Terasaki, T.; Joo, H.; Ryoo, R. *J. Phys. Chem. B* **2002**, *106*, 1256–1266.

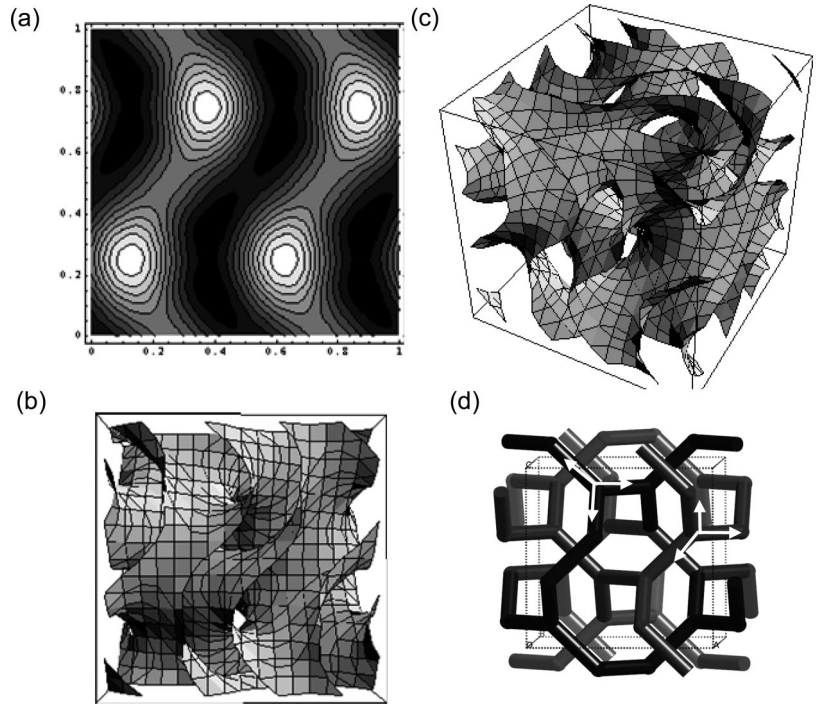

Figure 7. (a) Electrostatic potentials map in the section parallel to the (010) plane at $y = 0$, (b, c) 3D reconstructed structures obtained by EC corresponding to S85m sample, (b in the [100] direction and c close to the [111] direction), and (d) schematic representation of $Ia\bar{3}d$ structure. The arrows indicate the 3D channels, which increase the ionic/molecular interchange with the environment.

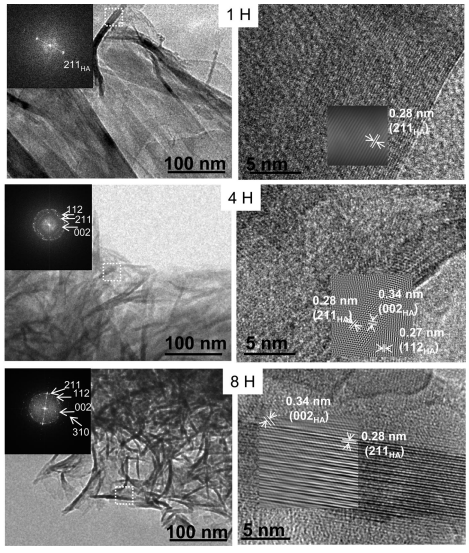

Figure 8. TEM images of S85m after being soaked in SBF at different times: 1 h in SBF. Needle-shaped crystallites are observed together with ACP grains. High-magnification image evidence ordered planes corresponding to (2 1 1) of an apatite phase; 4 h in SBF. Higher amount of polycrystalline apatite is observed onto the S85m surface. FT pattern and high-magnification image show the planes (1 1 2), (2 1 1), and (0 0 2), corresponding to an apatite phase; 8 h soaked in SBF. Most of the CaP observed correspond to needle-shaped Ca-deficient apatite.

in SBF (Figures 8e,f) S85m is fully covered by nanocrystalline Ca- deficient apatite with well-defined needle-shaped crystallites. To understand this superior bioactive behavior in 3D cubic mesoporous glass (S85m), we show a schematic representation of $Ia\bar{3}d$ structure (Figure 7d). This structure has a 3D bicontinuous network comprising a pair of rods (drawn in black and gray) mutually intertwined, creating the pore system available in three dimensions (the arrows indicate the 3D channels that comprise the pore). This 3D pore system provides not only high surface area and porosity but also easier interchange of ions, increasing mass transport, and diffusion processes. S85m shows the best crystalline apatite rate formation because of its excellent textural properties and structural characteristics. Cubic MBGs are able to nucleate biomimetic apatite without releasing high Ca^{2+} amounts and, therefore, without significantly increasing the pH of the environment.[12] The high mass transport, surface area, and pore volume in the mesoporous scale reduce the apatite nucleation time, although lower amounts of biomimetic calcium phosphate are obtained when compared with compositions with high CaO content.

Conclusions

In this work, we have presented mesoporous bioceramics exhibiting calcium phosphate nucleation and evolution that accurately mimic the in vivo bone mineral maturation. Depending on the chemical composition and the derived mesostructure, the MBG can also exhibit accelerated bioactivity that emerges from the textural properties. Ordered mesoporous bioactive glasses with 2D hexagonal structure and high calcium content have shown the first evidence of ACP−OCP−CDHA maturation stages as biomineralization governing mechanism, which have been described as a real mechanism in biological apatites. HRTEM studies performed on MBG materials after soaking in SBF have allowed us to monitor such biomineralization process.

The possibility of tailoring the structural characteristics of MBGs have allowed to obtain bioceramics with 3D cubic

bicontinuous structure, which exhibit higher accessibility to the diffusion process in pore systems leading to the most accelerated bioactive response until now described. Thanks to the 3D reconstruction performed on the mesoporous bioactive glasses by the electron crystallography technique, it has been possible to have a high knowledge of structural characteristics leading to a high understanding on the reactivity response in vitro.

Acknowledgment. Financial support of CICYT Spain, through research projects MAT2005-01486 and CAM S-0505/MAT/000324 is acknowledged.

Supporting Information Available: Additional information and two figures (PDF). This material is available free of charge via the Internet at http://pubs.acs.org.

CM800172X